3D reconstruction of surface cracks using bi-frequency eddy current images and a direct semi-analytic model

Caifang Cai, Thierry Bore, Florentin Delaine, Nicolas Gasnier, Eric Vourc'H

3D reconstruction of surface cracks using bi-frequency eddy current images and a direct semi-analytic model

IOP Conf. Series: Journal of Physics: Conf. Series **904** (2017) 012019 doi:10.1088/1742-6596/904/1/012019

3D reconstruction of surface cracks using bi-frequency eddy current images and a direct semi-analytic model

Caifang Cai[1], Thierry Bore[2], Florentin Delaine[3], Nicolas Gasnier[3], Eric Vourc'h[3]

[1]L2S, CentraleSupelec/CNRS/Université Paris-sud/Université Paris-Saclay, France
[2]School of Civil Engineering, University of Queensland, St Lucia, Australia
[3]SATIE, ENS Paris-Saclay /Université Paris-Saclay /CNRS, France
E-mail: eric.vourch@satie.ens-cachan.fr, bore.thierry@gmail.com, caifang.cai@l2s.centralesupelec.fr, romain.soulat@thalesgroup.com

Abstract. We propose a method for reconstructing 3D surface cracks in metallic parts form eddy current (EC) images. To do so, we use a semi-analytic direct model for representing the interactions between EC and a crack. In order to cope with the inverse problem consisting in reconstructing 3D cracks, we propose the use of a genetic algorithm based on the computation of bi-frequency EC images. Numerical experiments are carried out in order to analyze the performance of the reconstruction method for different signal to noise ratios. Moreover, the results obtained with a bi-frequency genetic algorithm are compared to those obtained with a mono-frequency algorithm.

Introduction

The non destructive evaluation (NDE) is an important issue for the industries submitted to high security and reliability requirements, such as the nuclear and aeronautic industries. It is in particular necessary to make sure that the metallic parts of the plants or of the aircrafts do not feature corrosion or cracks, whether at the manufacturing step or during the use of the part. Ultrasounds [1] and eddy currents (EC) [2] are the most widely used NDE techniques. The latter, which we consider in this paper, has the advantage of being sensitive to the defects mentioned above, while being easy to implement and robust. Beyond the detection of defects, the evaluation of their features is necessary. Indeed, accurately evaluating defects dimensions makes it possible to envisage appropriate reparation and optimization of the maintenance operation. EC NDE is still focusing a lot of research works. The ill posed nature of the inverse problem being part of the issues to overcome [3-5]. Apart from carrying out precise defects reconstruction, it is also important to design inversion methods featuring a reasonable computation time.
The inversion of EC signals can be envisaged considering total variation regularization methods [6], fast interpolation models (like meta-models obtained from databases) and the estimation of a restricted number of parameters characterising the shape of the defects [7]. Since a main difficulty of the inversion relies on the establishment of a confidence criterion on the results of the algorithm, statistical approaches (such as Markov chain Monte Carlo [8]) also are considered. Of course, they require a high number of resolutions of the direct problem. Non-iterative algorithms also are proposed based on punctual tests of the inspected structure with near real-time NDE applications in view [9].

In order to deal with an NDE problem, it is useful combine an experimental set-up and a signal processing technique designed to match each other as well as the kind of problem that is considered (geometry of the inspected part, kind of defects...). Regarding EC techniques one can distinguish two main types of experimental approaches: those implementing either pulsed EC [10] or on harmonic EC [11].
In this paper, we consider the EC systems for which the excitation is harmonic and the current distribution is uniform [12, 13]. Indeed, such a configuration is sensitive to the presence of cracks and generates a significant magnetic field component perpendicular to the surface of the part. In addition, in order to dispose of information relating to the 3 dimensions (3D) of the inspected part, we consider multi-frequency imagery systems. Indeed, an image, which consists in a cartography of the magnetic field component normal to the surface of the part, provides with 2D information. On the other hand, given the skin effect, the measurement of images for different excitation frequencies facilitates the discrimination of the information relative to the depth of the part.
Moreover, it has been demonstrated that a semi-analytic modeling approach such as the distributed point source method (DPSM) enabled building a direct model suitable for representing the interactions between a crack and uniform EC flows [13]. This direct model featuring a rather fast computation time, the reconstruction of cracks by means of an iterative algorithm based on the computation of EC images can be envisaged [14]. Such an approach was previously carried out considering the reconstruction of 2D surface cracks from mono-frequency EC images [15].
In this paper, we propose the extension of this method to the reconstruction of 3D surface cracks based on the use of bi-frequency EC images.
This paper is organized as follows: in section 2, we describe the EC bi-frequency imaging configuration which we consider and we remind the main points of the direct semi-analytic model to be applied to this configuration. In section 3, we propose an approach for solving the inverse problem consisting in reconstructing 3D surface cracks by means of a genetic algorithm (GA) [16] operating in a bi-frequency configuration. In section 4, we analyze the estimation performances provided by this algorithm and we compare them to a similar approach using only mono-frequency images.

EC configuration and direct model

The EC configuration we consider corresponds to a uniform EC flow [12, 13] perpendicular to the largest surface of a crack present in a metallic part. Such a choice enables maximizing the interactions between the EC and the crack and subsequently generating a significant magnetic field distribution $\boldsymbol{b}_z$ perpendicularly to the surface of the part (Figure 1). Note that in practice, if the crack direction is not a priori known, one may try and maximize $\boldsymbol{b}_z$ by optimizing the orientation of the inducer generating the EC. As the EC distribution is subject to the skin effect, the EC intensity decreases exponentially as the depth z increases. Moreover, the skin depth δ, which represents an approximation of the penetration depth of the EC within the part, vary as the inverse of the root mean square of the excitation frequency f:

$$\delta = 1/\sqrt{\pi f \sigma \mu_0 \mu_r} \qquad (1)$$

where μ_0 is the magnetic permeability in a vacuum, μ_r is the relative magnetic permeability and σ is the electric conductivity of the medium.
Therefore, the measurement of EC images (that is of 2D $\boldsymbol{b}_z$ cartographies at the surface of the part) at different frequencies provides with information relating to the 3 dimensions of the part which can be useful with a view to the 3D reconstruction of cracks.
We have previously proposed a direct model suitable for the configurations described above [13-15]. $\boldsymbol{b}_z$ is computed as the sum of the contributions of sources radiating according to Green's functions. The sources, which are placed at the metal/air interface and within the crack volume, take both the skin effect and the boundary conditions into account. The model thus requires a discretization of the volume of the metallic part and of the interface. Note that for the sake of accuracy of the modeling it is

suitable that the interface be meshed respecting a distance between the sources lower than a third of the characteristic distance of the electromagnetic problem, which is typically in the order of the skin depth δ. The model, which is based on the assumption that the presence of a crack represents a small perturbation with respect to a sound volume [17], has been previously validated by comparison to finite elements simulations and measurements [13].

Figure 1 provides with bi-frequency images computed with the model. They correspond to the case of an aeronautic aluminum alloy such that $\sigma = 17.6$ MS.m^{-1} and $\mu_r = 1$ and featuring a crack of width, length and depth W_x, L_y and D_z equal to 1 mm, 4 mm and 5 mm respectively.

These images correspond to f =100 Hz and f = 1200 Hz EC frequencies, which corresponds to 12.6 mm et 3.6 mm skin depths respectively. The main parameters of the model, such as those regarding the distretization of the workspace, are provided in Table 1. The same parameters will be used for every simulations reported in the paper.

Table 1. DPSM direct model configuration.

	x dimension		y dimension		z dimension	
	(mm)	(pixels)	(mm)	(pixels)	(mm)	(pixels)
Active sources planes (metal)	10	$n = 20$	10	$n = 20$	6	$p = 12$
b_z cartography	54	$m = 40$	54	$m = 40$		
Interface sources plane	@ f = 100 Hz			@ f = 1200 Hz		
	x and y dimensions			x and y dimensions		
	(mm)	(Pixels)		(mm)	(Pixels)	
	$\cong 4$	$q = 13$		$\cong 1$	$q = 45$	

Given the symmetry of the EC problem, the images feature two lobes and are symmetrical with respect to the x axis (Figure 1). It is to be noted that the higher frequency image, which carries information mostly regarding the top of the crack, features a lower spatial spread than the lower frequency image, which carries information regarding a deeper volume of the structure. According to this typical result, in an inversion algorithm the use of high frequency images should contribute to precisely estimate the parameters W_x, L_y , while that of low frequency images are due to improve the estimation of D_z.

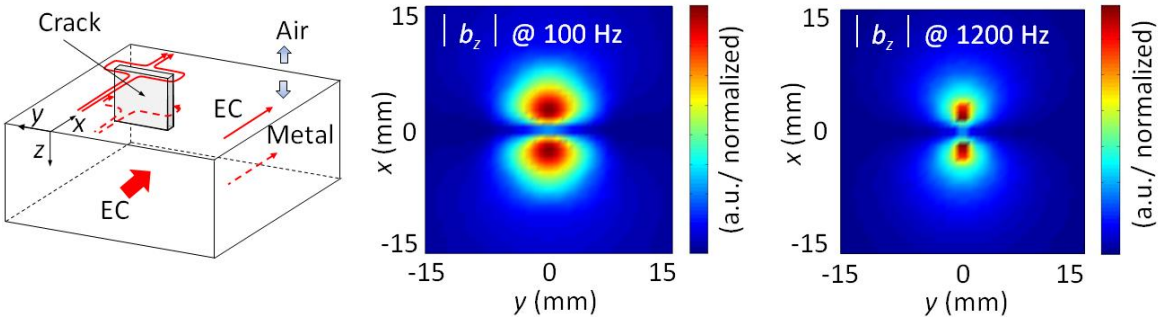

Figure 1. Interactions between a uniform EC flow and a 3D crack featuring a parallelepiped shape; synthetic $|\boldsymbol{b}_z|$ images at 100 Hz and 1200 Hz, for a metallic part featuring $\sigma = 17.6$ MS.m^{-1} and $\mu_r = 1$ and for a crack such that $\{W_x = 1$ mm, $L_y = 4$ mm, $D_z = 5$ mm$\}$.

Inverse problem

The accuracy and computational efficiency of the direct model described in section 2 [13-15] led us to design an iterative crack reconstruction algorithm relying on the comparison of EC images computed with this model. In addition, according to the reasons given in section 2, with 3D crack reconstruction in view, the algorithm should use images at different frequencies.
Due to the complexity of the EC problem, different cracks are likely to provide with close EC images. Therefore, rather than an algorithm based on a gradient method, we chose to design a genetic algorithm (GA). Indeed, thanks to random variations of the features of the tested cracks at each iteration (mutation operation), the GA minimizes the risk to converge towards a local minimum.

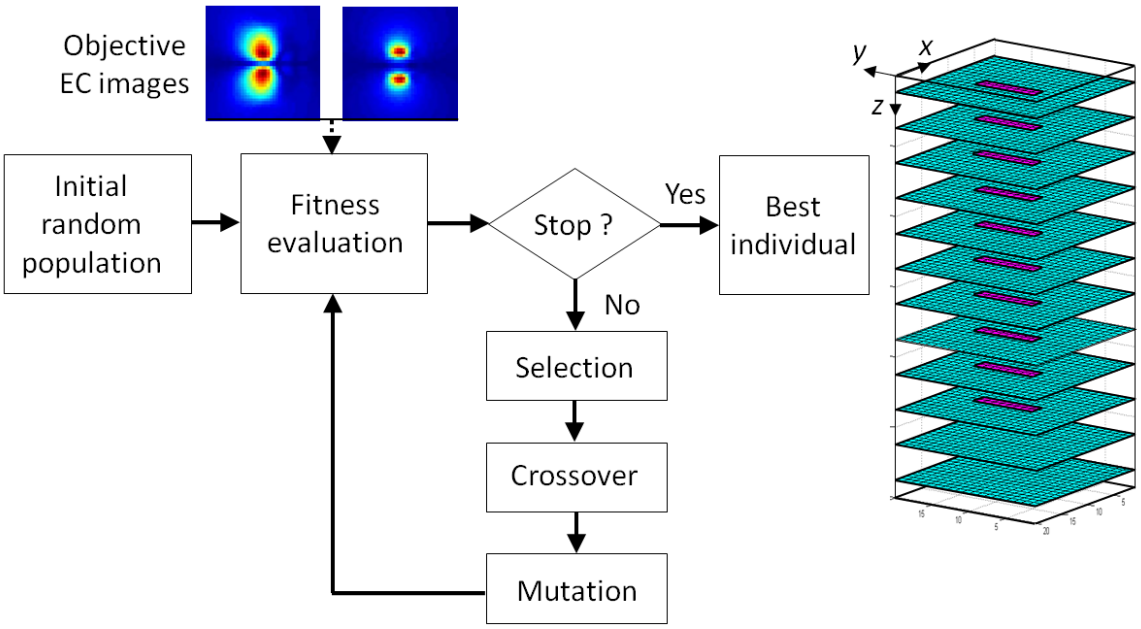

Figure 2. Genetic algorithm architecture for the reconstruction of 3D surface cracks from bi-frequency EC images.

The architecture of the GA is described in Figure 2. It uses a population of 8 individuals (cracks). The latter is randomly initialized while ensuring a minimum fitness of each individual. It is to ne noted that the population size was not optimized for minimizing the number of iterations, but simply chosen as 8. At each iteration, the fitting between bi-frequency EC images of the individuals and reference images corresponding to the researched crack is evaluated. Images comparison is carried out according to a normalized weighted relative square error ε_{wrse}, which gives all the more weight to a pixel that its energy is high. Let us denote $\boldsymbol{b_z} \in \mathbb{C}^M$ the vertical magnetic field at the surface of the metallic structure, where $M = m \times m$ is the image (i.e. cartography) dimension. ε_{wrse}, which is a relative error between $\boldsymbol{b_z}$ and a reference $\boldsymbol{b_{z0}}$ (output of the researched crack) is defined as follows:

$$\varepsilon_{wrse} = \frac{[\boldsymbol{b_z}-\boldsymbol{b_{z0}}]' W [\boldsymbol{b_z}-\boldsymbol{b_{z0}}]}{\boldsymbol{b_{z0}}' W \boldsymbol{b_{z0}}} \qquad (2)$$

where $W = diag|\boldsymbol{b_{z0}}|$ is the diagonal matrix supporting $|\boldsymbol{b_{z0}}|$ on the diagonal. In (2), the normalization is performed with respect to the total energy (or weighted energy) of the reference $\boldsymbol{b_{z0}}$.

The bi-frequency fitting criterion is based on the sum of the squares of the mono-frequency ε_{wrse} (such a sum proved more efficient than a product as regards the convergence of the algorithm).
Once evaluated, the population is modified in 3 steps: (i) selection (by means of a fortune wheel), (ii) crossover between the individuals and (iii) mutation: the 3 dimensions W_x, L_y et D_z of the individuals randomly mute according to given Gaussian laws.

Genetic algorithm performance analysis

GAs such as described in section 3 have been implemented in order to reconstruct cracks of dimensions such that $\{0.5\text{ mm} \le W_x \le 10\text{ mm},\ 0.5\text{ mm} \le L_y \le 10\text{ mm}\ 0.5\text{ mm} \le D_z \le 6\text{ mm}\}$. The used EC frequencies are f =100 Hz and f = 1200 Hz. This choice is a trade off providing δ skin depths adapted to the considered cracks depths and to a meshing condition (the interface sources must be spaced out of a distance lower than $\delta/3$) compatible with a fast computation time of the direct model.
Here we report on the performances of 3 different GAs: on the one hand 2 mono-frequency GAs using images at 100 Hz and 1200 Hz respectively, on the other hand a bi-frequency GA using images at both these frequencies. Numerical experiments have been carried out for 4 signal to noise ratios (SNR) comprised between 3 and 10 dB. 10 dB being a typical SNR of EC experimental systems.
Figures 4 and 5 compare the estimation performance of theses algorithms in the case of 2 cracks featuring the same width W_x = 1 mm and length L_y = 4 mm, but different D_z depths equal to 1 mm and 5 mm respectively (Figure 3). Each point of the convergence statistics reported in Figures 4 and 5 results from 30 drawings of the corresponding GA, the number of iterations being fixed at 30 per drawing which guaranties the GA to converge, according to our experience.

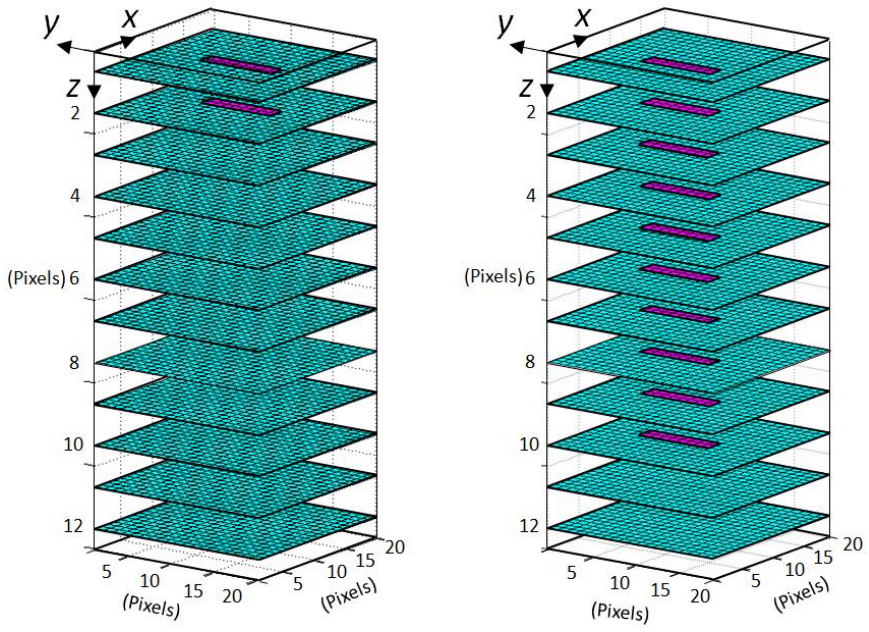

Figure 3. (a) Crack corresponding to the simulations reported in Figure 4 $\{W_x = 1\text{ mm}, L_y = 4\text{ mm}, D_z = 1\text{ mm}\} \Leftrightarrow \{W_x = 2$ pixel, $L_y = 8$ pixels, $D_z = 2$ pixels$\}$; (b) crack corresponding to the simulations reported in Figure 5 $\{W_x = 1\text{ mm}, L_y = 4\text{ mm}, D_z = 5\text{ mm}\} \Leftrightarrow \{W_x = 2$ pixel, $L_y = 8$ pixels, $D_z = 10$ pixels$\}$. The discretization of the DPSM direct model is as described in Table 1.

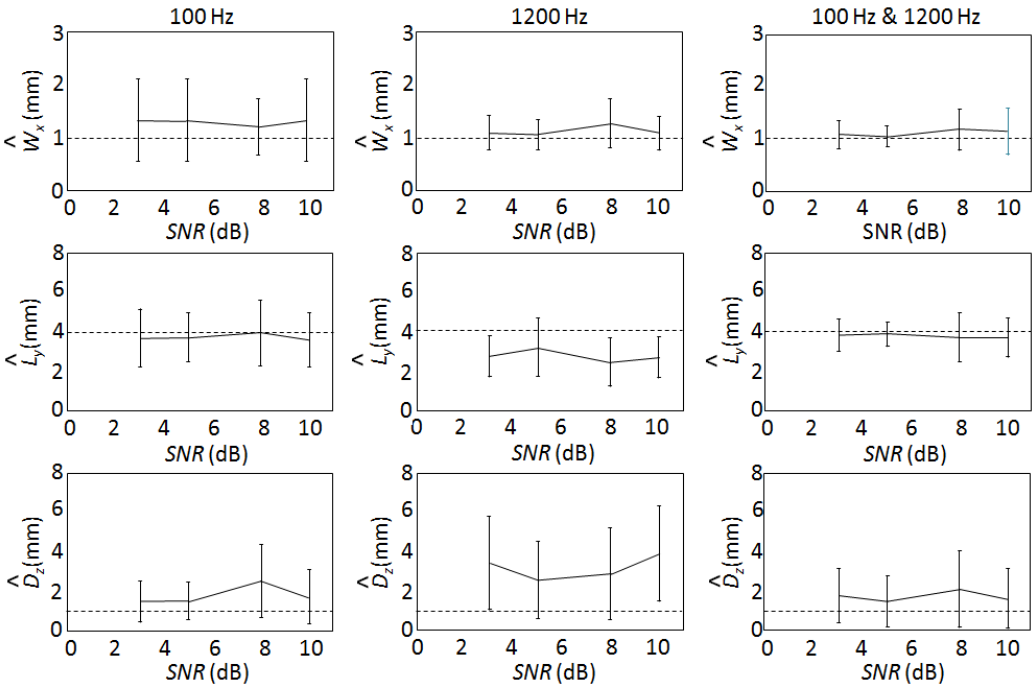

Figure 4. Expectancy and standard deviation of $\widehat{W_x}$ and $\hat{L}_y$ *and* $\widehat{D_z}$ for 30 drawings of mono-frequency and bi-frequency GAs operating at 100 Hz and 1200 Hz with 30 iterations. Features of the researched crack: $\{W_x = 1 \text{ mm}, L_y = 4 \text{ mm}, \ D_z = 1 \text{ mm}\} \Leftrightarrow \{W_x = 2 \ \text{ pixel}, L_y = 8 \ \text{ pixels}, D_z = 2 \text{ pixels}\}$.

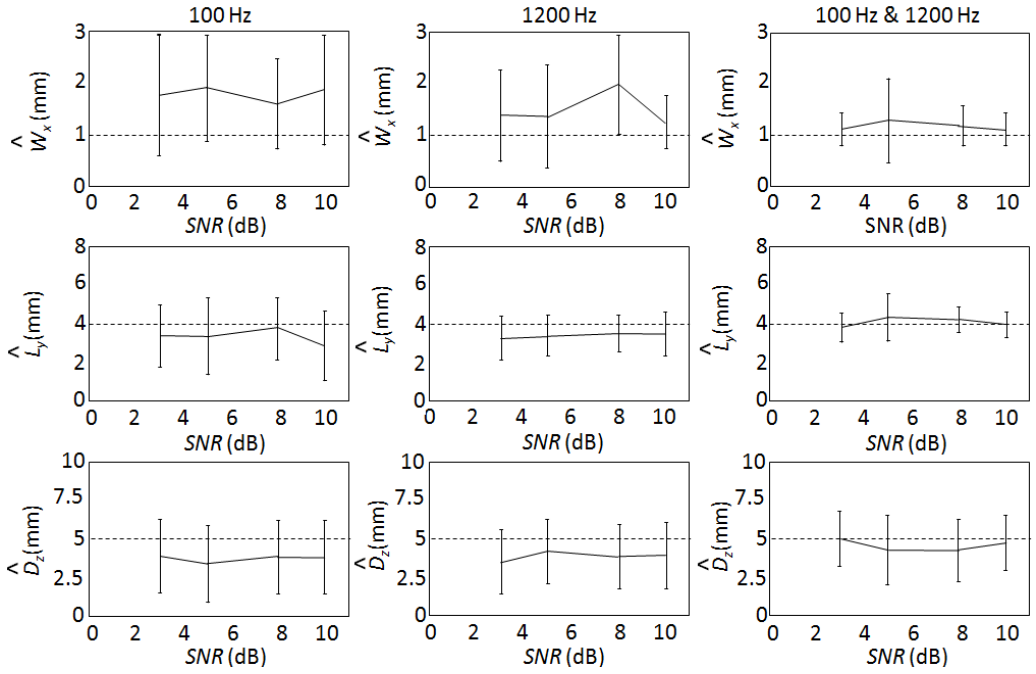

Figure 5. Expectancy and standard deviation of $\widehat{W_x}$ and $\hat{L}_y$ *and* $\widehat{D_z}$ for 30 drawings of mono-frequency and bi-frequency GAs operating at 100 Hz and 1200 Hz with 30 iterations. Features of the researched crack: $\{W_x = 1 \text{ mm}, L_y = 4 \text{ mm}, \ D_z = 5 \text{ mm}\} \Leftrightarrow \{W_x = 2 \ \text{ pixel}, L_y = 8 \ \text{ pixels}, D_z = 10 \text{ pixels}\}$.

As regards of the results reported in Figure 4, it is to be noted that the mono-frequency GA at 100 Hz is the one providing the less accurate $\widehat{W_x}$ estimate, with an average bias lower than 0.5 mm (1 pixel) and a standard deviation in the order of 1 mm. The mono-frequency GA at 1200 Hz provides with poor accuracy of $\widehat{D_z}$, with a bias and a standard deviations of about 2 mm, whatever the SNR. Such results can be attributed to the spatial spread of low frequency images and to the small skin depth of EC at higher frequency, as mentioned in section 2.
As far as the bi-frequency GA is concerned, precise estimation of the three dimensions of the crack is carried out, whatever the SNR.
Regarding the reconstruction of the deeper crack (Figure 5), the mono-frequency GA at 100 Hz once again lacks accuracy in the $\widehat{W_x}$ estimation, and so does the GA at 1200 Hz. Regarding $\widehat{D_z}$, a bias in the order of 1 mm is observed with both the mono-frequency GAs. Such a result reveals the ill-posed nature of EC problems.
As far as the bi-frequency GA is concerned, accurate estimation of the 3 dimensions of the deeper crack is also carried out, the bias being close to zero for a 10 dB SNR.
These results go to prove that the proposed approach, consisting in a GA implementing bi-frequency EC images provided by the semi-analytic DPSM based model, is suitable for accurately reconstructing 3D surface cracks. Moreover, this method is rather computationally efficient, a drawing of such an algorithm requiring a computation time in the order of several minutes when implemented by means of Matlab™ on a 3.4 GHz PC.

Conclusion

In this paper, a method operating in bi-frequency applying to systems featuring homogeneous EC induction has been proposed for reconstructing 3D surface cracks. This method is an iterative approach relying on the use a semi-analytic direct model of EC images. With a view to enable the estimation of the depth of the cracks, bi-frequency EC images taking the skin effect into account have been used. The proposed method has been implemented in the form of a GA. Numerical experiments including comparison to mono-frequency GAs have been carried out for different SNR. The bi-frequency approach proved more efficient, and led to accurate estimation of the 3 dimensions of cracks even at low SNR.
Based on these results the 3D reconstruction of buried cracks can be envisaged. Therefore, further works will focus on a multi-frequency approach taking the skin effect into account. The application of the method to experimental data will also be considered.

References

[1] Kubinyi M, Docekal A, Ramos H and Ribeiro A 2010 *Przegląd Elektrotechniczny* **86** 249-254
[2] Bernieri A, Ferrigno L, Laracca M and Molinara M 2008 *Instrumentation and Measurement, IEEE Transactions on* **57**(9) 1958-1968
[3] Colton D and Päivärinta L 1992 *Archive for rational mechanics and analysis* **119**(1), 59-70
[4] Isakov, V. 1993 *Inverse Problems* **9**(6) 579
[5] Yamamoto M 1997 *International Journal of Applied Electromagnetics and Mechanics* **8**(1) 77-98
[6] Ribeiro A L, Ramos H G, Pasadas D and Rocha T 2014, February *40th Annual Review Of Progress In Quantitative Nondestructive Evaluation AIP Publishing* **1581(**1) 1428-1432
[7] Douvenot R, Lambert M and Lesselier D 2011 April Magnetics, *IEEE Transactions on* **47(**4) 746-755
[8] Cai C, Rodet T and Lambert M 2014 *Journal of Physics: Conference Series*, IOP Publishing **542(**1) 012009
[9] Tamburrino A, Calvano F, Ventre S. and Rubinacci G 2012 *NDT & E International* **47** 26-34.

[10] Tian, G. Y., Sophian, A. Taylor, D. and Rudlin, J 2005. *IEEE Sensors Journal*, *5*(1), 90-96.
[11] Ribeiro, A L, Ramos, H G, & Arez, J C 2012. Measurement, 45(9), 2246-2253.
[12] Koyama K, Hoshikawa H and Taniyama N 2000, October *Proceedings of WCNDT*
[13] Thomas V, Joubert P Y, Vourc'h E and Placko D 2010, February *Sensors Applications Symposium (SAS IEEE)* 154-157
[14] Placko D, Bore T and Kundu T 2012 *Ultrasonic and Electromagnetic NDE for Structure and Material Characterization: Engineering and Biomedical Applications CRC Press* 249-294
[15] Vourc'h E, Bore T, Cai C and Soulat R 2015 *Journal of Physics: Conference Series*, 657(1), 012015.
[16] Goldberg D E and Holland J H 1988 *Machine Learning, Kluwer Academic Publishers* **3**(2-3), 95-99.
[17] Sabbagh H and Sabbagh L 1986 *Magnetics, IEEE Transactions on* **22**(4) 282-291